research papers

Maximum entropy method and charge flipping, a powerful combination to visualize the true nature of structural disorder from *in situ* X-ray powder diffraction data

Ali Samy,^{a}‡ Robert E. Dinnebier,^{a}* Sander van Smaalen^b* and Martin Jansen^a

^{a}Max Planck Institute for Solid State Research, Heisenbergstrasse 1, D-70569 Stuttgart, Germany, and ^{b}Laboratory of Crystallography, University of Bayreuth, D-95440 Bayreuth, Germany

‡ Deceased.

Correspondence e-mail:
r.dinnebier@fkf.mpg.de,
smash@uni-bayreuth.de

In a systematic approach, the ability of the Maximum Entropy Method (MEM) to reconstruct the most probable electron density of highly disordered crystal structures from X-ray powder diffraction data was evaluated. As a case study, the ambient temperature crystal structures of disordered α-$Rb_2[C_2O_4]$ and α-$Rb_2[CO_3]$ and ordered δ-$K_2[C_2O_4]$ were investigated in detail with the aim of revealing the 'true' nature of the apparent disorder. Different combinations of F (based on phased structure factors) and G constraints (based on structure-factor amplitudes) from different sources were applied in MEM calculations. In particular, a new combination of the MEM with the recently developed charge-flipping algorithm with histogram matching for powder diffraction data (pCF) was successfully introduced to avoid the inevitable bias of the phases of the structure-factor amplitudes by the Rietveld model. Completely *ab initio* electron-density distributions have been obtained with the MEM applied to a combination of structure-factor amplitudes from Le Bail fits with phases derived from pCF. All features of the crystal structures, in particular the disorder of the oxalate and carbonate anions, and the displacements of the cations, are clearly obtained. This approach bears the potential of a fast method of electron-density determination, even for highly disordered materials. All the MEM maps obtained in this work were compared with the MEM map derived from the best Rietveld refined model. In general, the phased observed structure factors obtained from Rietveld refinement (applying F and G constraints) were found to give the closest description of the experimental data and thus lead to the most accurate image of the actual disorder.

1. Introduction

Rietveld refinement is considered to recover the maximum amount of information that is contained in powder diffraction data (David *et al.*, 2002). Nevertheless, this amount is smaller than that contained in a complete set of observed structure-factor amplitudes (van Smaalen, 2007). The correlations between the different crystallographic parameters as well as the application of constraints and restraints is often unavoidable in Rietveld refinement. In the case of an ordered crystal structure, the refinement process is able to reconstruct the phases of structure factors with reasonable accuracy even if the structure model is not perfect. However, if the crystal is disordered (except for simple cases) the refinement process is not easy, typically requiring the introduction of rigid bodies, constraints, restraints and anharmonic anisotropic displacement parameters (a.d.p.s) to reach convergence. In such cases the structural model obtained from Rietveld refinement needs to be verified and improved. This can be achieved by the

Maximum Entropy Method (MEM), which can be used as a complementary method for deriving the most probable electron density from limited information by maximizing the entropy. Recent progress in synchrotron powder X-ray diffraction techniques, including third generation synchrotron sources, low-noise image-plate detectors (IP), new optical systems and analytical methods, enables the extraction of structure-factor amplitudes with high accuracy. These developments not only increase the success rate of crystal structure determination from powder diffraction data, but also (by determining the charge-density distribution using the MEM) allow for the investigation of advanced structural features such as disorder, diffusion pathways in ionic conductors, electron density due to chemical bonds and nano-applications (Dinnebier *et al.*, 1999; Yashima & Tsunekawa, 2006; Takata, 2008).

However, the reconstruction of accurate electron density from experimental data suffers from model biasing effects in addition to the artifacts caused by the incompleteness of the data set. The dependence of MEM electron densities on the lack of completeness of the underlying data set was studied by Takata & Sakata (1996), and Yamamoto *et al.* (1996). Efforts have been undertaken to overcome these limitations by introducing alternative weighting factors that force the distribution of the residuals of the final structure factors towards the required Gaussian distribution (*e.g.* de Vries *et al.*, 1994; Palatinus & van Smaalen, 2002). In particular for powder diffraction data, severe overlapping (where only the sum of the individual intensities of the overlapping peaks is available) can be handled using so-called *G* constraints (Sakata *et al.*, 1990), thus avoiding a model bias due to the separation of the measured intensity into contributions from the reflections belonging to this overlap group. The combination of the MEM and Rietveld methods was introduced by Takata *et al.* (1995) and is called the REMEDY cycle, after the name of the computer program. In this method, the structure model is iteratively improved by replacing the values of the calculated structure factors (F_{calc}) from Rietveld refinement by the corresponding values of the observed structure factors F_{obs} obtained from MEM calculations.

Here we present a new combination of the MEM and the method of charge flipping (Oszlányi & Sütő, 2004, 2005, 2007; Palatinus, 2004). Reflection phases from charge flipping were introduced for two purposes: first to improve the accuracy of the phases obtained from the Rietveld method and second as a fast method to visualize the type of disorder independent of the Rietveld model. This approach not only succeeded in revealing the basic features of the crystal structure, but also fine details as the type of disorder (rotational and/or conformational disorder) and the type of thermal vibrations. In general, different types of structure-factor amplitudes and phases imposing different types of constraints were subjected to the MEM with the aim of acquiring the least biased electron density in order to visualize and understand the disorder of α-$Rb_2C_2O_4$ and α-Rb_2CO_3 (Dinnebier *et al.*, 2005). For comparison between the different MEM maps, the difference MEM maps [$\rho_{(I)}^{MEM} - \rho_{calc}^{MEM}$], where (I) refers to F_{obs}, $F_{obs} + G$

constraints, $F_{LeBail} + G$ constraints, CF + $F_{LeBail} + G$ constraints and CF + $F_{obs} + G$ constraints, were calculated and visualized in three- and two-dimensional space, in addition to calculations of the agreement factors and the volume and area of the enclosed surfaces.

It will be shown that charge flipping with structure-factor amplitudes obtained from a Le Bail fit is a powerful combination to reconstruct an approximate electron-density map of disordered materials by the MEM. In addition, G constraints are used to handle the overlapping reflection in the MEM calculation, and the histogram matching method is used for repartitioning the overlapping reflections in the pCF approach.

2. Methods

2.1. Maximum Entropy Method (MEM)

The concept of entropy was introduced in the field of crystallography to handle the series termination effects in Fourier maps. A perfect Fourier map would require a complete set of structure factors up to at least $(\sin \theta/\lambda)_{max} = 5.0 \text{ Å}^{-1}$ (de Vries *et al.*, 1996). In the case of the powder diffraction experiment, accessible information is limited compared with single-crystal data owing to the projection of the three-dimensional reciprocal space onto the one-dimensional 2θ axis and the resulting intrinsic and accidental peak overlap. The maximum entropy method (MEM) can be used to extract the maximum amount of information from a limited set of data by maximizing the entropy. The entropy of any trial density is defined relative to a prior density ρ^{prior} as

$$S = -\sum_{i=1}^{N_{pix}} \rho_i \ln(\rho_i/\rho_i^{prior}), \qquad (1)$$

where the electron density is sampled at the points of a $N_1 \times N_2 \times N_3 = N_{pix}$ grid over the unit cell. The prior density or prior can be a constant function, thus called a flat or uniform prior. Alternatively, it can represent any desirable distribution of the available electrons over the unit cell. A particularly useful prior is the procrystal density that is defined as the electron density corresponding to the indepedent atom model (IAM), as it is obtained, for example, from the best Rietveld refined structure model.

The goal of the MEM is to find the electron density that maximizes the entropy S subject to various constraints. The method of undetermined Lagrange multipliers is used to find the maximum of $Q = S - \lambda_N C_N - \lambda_F C_F - \lambda_G C_G$, with the Lagrange multipliers λ and the constraints C as defined below. According to $\partial Q/\partial \lambda = 0$, the maximum is reached when the different constraints C_N, C_F and C_G are all zero. All constraints are functions of the electron density. The first constraint is the normalization of the electron density and it is defined as

$$C_N = N_{el} - \frac{V}{N_{pix}} \sum_{i=1}^{N_{pix}} \rho_i = 0, \qquad (2)$$

Ali Samy *et al.* · Maximum entropy method and charge flipping **185**

where N_{el} is the number of electrons in the unit cell of volume V. λ_N can be eliminated from the MEM equations and does not appear in the iterative procedure. The prior obeys the same normalization; the density of the flat prior thus is $\rho_i = N_{el}/V$. The second constraint C_F is based on the phased observed structure factors F_{obs} and is defined as

$$C_F = -1 + \frac{1}{N_F}\sum_{i=1}^{N_F} w_i \left(\frac{|F_{obs}(\mathbf{H}_i) - F_{MEM}(\mathbf{H}_i)|}{\sigma(\mathbf{H}_i)}\right)^2 = 0, \quad (3)$$

where N_F is the number of isolated phase observed structure factors $F_{obs}(\mathbf{H}_i)$ with standard uncertainties $\sigma(H_i)$; $F_{MEM}(\mathbf{H}_i)$ are the phased structure factors obtained by Fourier transform of the trial electron density (ρ_i); w_i is the weight factor (its value is unity if no weights are applied).

Overlapping reflections in powder diffraction are managed in the MEM by applying the so-called G-constraint (Sakata *et al.*, 1990), defined as

$$C_G = -1 + \frac{1}{N_{all}}\sum_{i=1}^{N_F} w_i \left(\frac{|F_{obs}(\mathbf{H}_i) - F_{MEM}(\mathbf{H}_i)|}{\sigma(\mathbf{H}_i)}\right)^2$$
$$+ \frac{1}{N_{all}}\sum_{j=N_F+1}^{N_{all}} \left(\frac{G_{obs}^j - G_{MEM}^j}{\sigma(G_{obs}^j)}\right)^2 = 0, \quad (4)$$

where N_G is the number of overlap groups and

$$G^j = \sum_{k=1}^{N_G(j)}\left(\frac{m_k}{\sum m_k}|F(H_K)|^2\right)^{1/2} \quad (5)$$

with the multiplicity m_k of the reflection k. $N_G(j)$ is the number of reflections contributing to the jth overlap group. The error propagation law is used to calculate the standard uncertainty of the group reflection according to

$$\sigma(G) = 1/G(j)\left[\sum_i \left(F_j\left(m_j/\sum m_k\right)\sigma(F_j)\right)^2\right]^{1/2}. \quad (6)$$

Convergence of the MEM can only be achieved if a sufficiently large fraction of the reflections is part of the F constraint (Sakata *et al.*, 1990). In our approach, a single Lagrange multiplier has been used for the combined F and G constraint defined as

$$C_{FG} = C_G = -1 + \frac{1}{N_F}\sum_{i=1}^{N_F} w_i \left(\frac{|F_{obs}(\mathbf{H}_i) - F_{MEM}(\mathbf{H}_i)|}{\sigma(\mathbf{H}_i)}\right)$$
$$+ \frac{1}{N_{all}}\sum_{j=N_F+1}^{N_{all}} \left(\frac{G_{obs}^j - G_{MEM}^j}{\sigma(G_{obs}^j)}\right) = 0 \quad (7)$$

where $N_{all} = N_F + N_G$.

The initial electron density or prior density ρ_i^{prior} can be introduced as a flat-prior, as in the present case for the
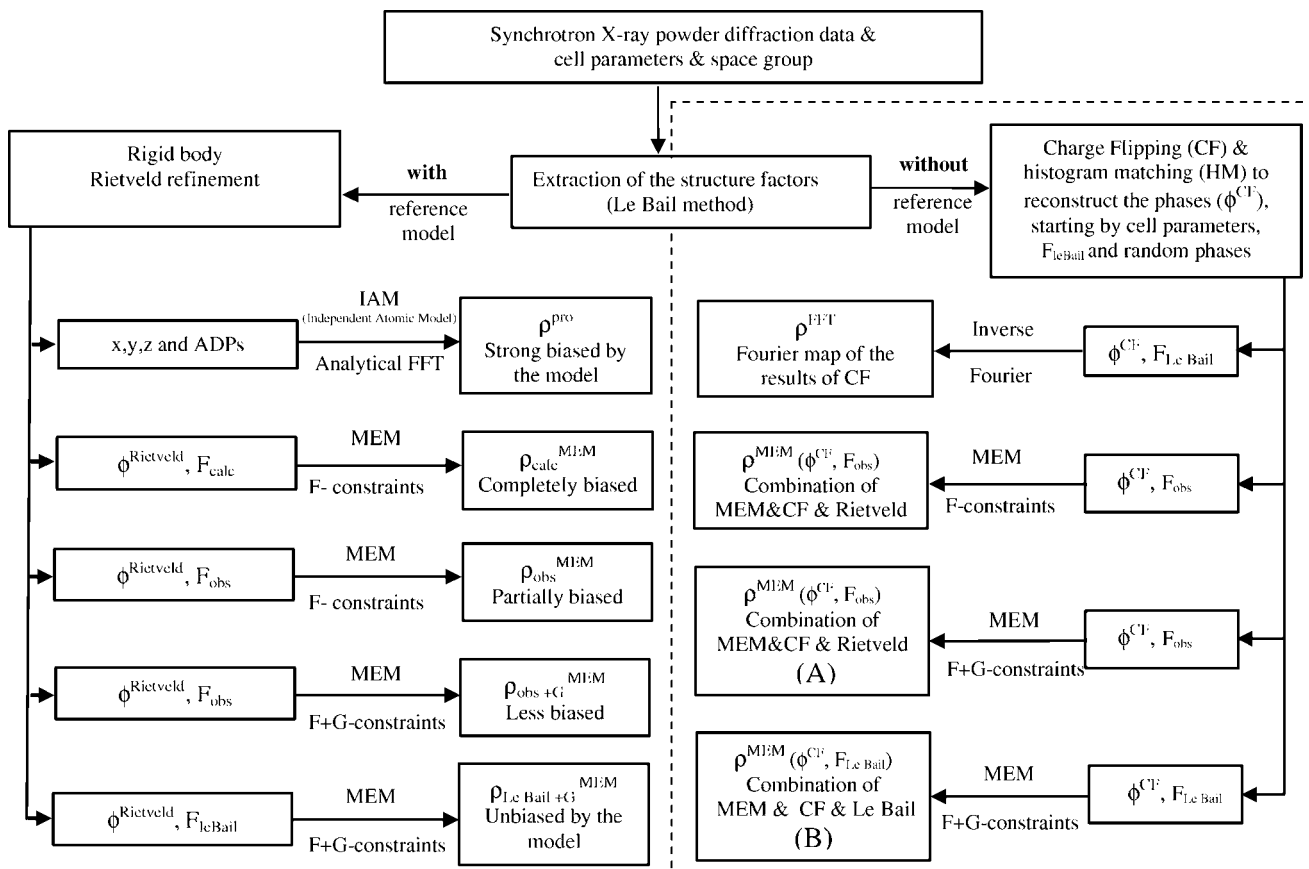

Figure 1
Flowchart showing the procedure for extracting the different types of structure factors and phases used to reconstruct the different types of electron-density maps from powder diffraction data. The procedure of the combination of MEM and CF is marked by a dashed line.

Table 1
Crystallographic information of α-Rb$_2$C$_2$O$_4$, α-Rb$_2$CO$_3$ and δ-K$_2$C$_2$O$_4$ as obtained from Rietveld refinements.

Chemical formula	α-Rb$_2$C$_2$O$_4$	α-Rb$_2$CO$_3$	δ-K$_2$C$_2$O$_4$
Space group	$P6_3/mmc$	$P6_3/mmc$	$Pbam$
Z	2	2	2
a (Å)	6.468 (18)	5.892 (24)	10.930 (28)
b (Å)	6.468 (18)	5.892 (24)	6.1284 (15)
c (Å)	8.255 (24)	7.796 (39)	3.4830 (9)
V (Å^3)	299.1 (16)	234.4 (20)	233.3 (17)
$F(000)$	236	208	164
Temperature (K)	683	873	295
Wavelength λ (Å)	0.9224 (2)	0.9224 (2)	0.9224 (2)
$(\sin\theta/\lambda)_{max}$	0.78630	0.78630	0.78630
No. of unique reflections	40	39	68
No. of group reflections	6	6	9
R_P	0.0105	0.0120	0.0138
R_{wp}	0.0139	0.0192	0.0183
GOF	0.79	0.98	1.10

description of disorder or in the case of anharmonic temperature vibrations when the exact position of the atoms is the quantity of interest. On the other hand, the procrystal is used as the prior density when the quantity of interest is the redistribution of electron density due to chemical bonds.

2.2. Charge flipping for powder (pCF)

Charge flipping is an algorithm that was recently proposed for *ab initio* structure determination from single-crystal and powder X-ray diffraction data (Oszlányi & Sütő, 2004, 2005; Palatinus, 2004; Baerlocher *et al.*, 2007). The method is based on an iterative procedure, whereby in each cycle density values smaller than some positive threshold δ values are given the opposite sign. The result is an electron-density map and a set of phases for the observed structure factors. With powder diffraction data, the Le Bail method can be used to extract the starting values of the structure-factor amplitudes. Histogram matching (Zhang & Main, 1990) can be used to repartition

overlapping reflections through the step of density modification. We have used this version of charge flipping (pCF) for the reconstruction of phases of structure factors (Baerlocher *et al.*, 2007).

2.3. Combination of the MEM and charge flipping

Much attention has been given to the model bias of the MEM. Both the values of the observed structure-factor amplitudes and the phases could be affected by the model, thus leading to biased electron densities. To overcome this problem, pCF is used to solve the phase problem. It is assumed that the structure-factor amplitudes have been extracted (using the Le Bail method or a similar algorithm). The reflection phases obtained by pCF can be combined with either the observed structure factors obtained from Rietveld refinement or the structure factors extracted from a Le Bail fit. In the first case the Rietveld model can be tested for phase biasing effects, while for the second case the resultant MEM map is considered completely unbiased by a structure model, since the phases and structure-factor amplitudes are obtained directly from the data. Uncertainties or model bias on amplitudes are removed by the use of combined F and G constraints together with phases from CF. In Fig. 1 the dashed outline refers to the procedure of MEM and CF; the two different combinations are designated by (A) and (B).

3. Experimental

3.1. X-ray powder diffraction

In situ X-ray powder diffraction data of potassium and rubidium oxalates and their corresponding carbonates as decomposition products were collected at high temperature using a wavelength of 0.9224 (2) Å in transmission geometry with a small hot environment cell at beamline X7B at the National Synchrotron Light Source (NSLS) at Brookhaven National Laboratory. The samples were contained in sealed quartz capillaries (diameter 0.5 mm). Details of the experimental setup as well as the description of the different crystal structures have been previously described (Dinnebier *et al.*, 2005). For the present study, three phases were selected: the highest-temperature phases α-Rb$_2$C$_2$O$_4$ and α-Rb$_2$CO$_3$, and the room-temperature phase δ-K$_2$C$_2$O$_4$. The δ phase of potassium oxalate crystallizes in the space group $Pbam$, with the ordered oxalate anion in planar conformation (Fig. 2c). The oxalate anions in the α phase of rubidium oxalate in the space group $P6_3/mmc$ are staggered and orientationally and conformationally disordered (Fig. 2a). Good Rietveld refinements are achieved assuming a
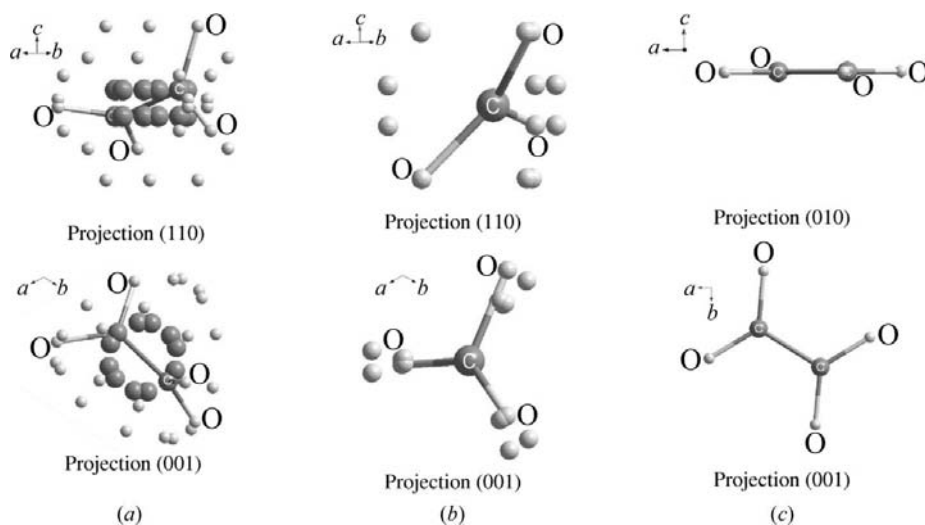
Figure 2
Two perspective projections each of the disordered oxalate and carbonate dianions of (a) α-Rb$_2$C$_2$O$_4$ and (b) α-Rb$_2$CO$_3$, and of the ordered, planar oxalate unit in (c) δ-K$_2$C$_2$O$_4$ dianions.

Ali Samy *et al.* · Maximum entropy method and charge flipping **187**

Table 2
Characteristics of the MEM calculations.

All calculations are based on the Sakata–Sato algorithm and a flat prior (§2.1).

Chemical formula	δ-K$_2$C$_2$O$_4$	α-Rb$_2$C$_2$O$_4$	α-Rb$_2$CO$_3$
Number of pixels	$108 \times 64 \times 36$	$96 \times 96 \times 108$	$54 \times 54 \times 72$
Pixel size (Å^3)	$0.101 \times 0.095 \times 0.096$	$0.067 \times 0.067 \times 0.076$	$0.109 \times 0.109 \times 0.108$
Electrons per unit cell	164	236	208
Lagrange multiplier λ	0.05	0.05	Automated
R_F/R_{wF} ($\rho_{F_{calc}}^{MEM}$)	0.00626/0.00351	0.0181/0.0054	0.0203/0.0051
R_F/R_{wF} ($\rho_{F_{obs}}^{MEM}$)	0.0066/0.0035	0.0236/0.0054	0.0174/0.0051
R_F/R_{wF}, R_G/R_{wG} ($\rho_{F_{obs}+G}^{MEM}$)	0.0073/0.0035, 0.0055/0.0042	0.0210/0.0050, 0.0332/0.0105	0.0180/0.0050, 0.0148/0.0127
R_F/R_{wF}, R_G/R_{wG} ($\rho_{F_{LeBail}+G}^{MEM}$)	0.0149/0.0117, 0.0208/0.0124	0.0329/0.0062, 0.0260/0.0077	0.0132/0.0052, 0.0277/0.0172
R_F/R_{wF}, R_G/R_{wG} ($\rho_{F_{LeBail}+CF+G}^{MEM}$)	0.0143/0.0118, 0.0176/0.0117	0.0373/0.0062, 0.0286/0.0085	0.0173/0.0049, 0.0305/ 0.0192
R_F/ R_{wF}, R_G/R_{wG} ($\rho_{F_{obs}+CF+G}^{MEM}$)	0.0057/0.0035, –/–	0.0217/0.0051, 0.0311/0.0097	0.0167/0.0052, 0.0041/0.0036
R (diff_$\rho_{F_{obs}}^{MEM}$)	0.029162	0.064700	0.05399
R (diff_$\rho_{F_{obs}+G}^{MEM}$)	0.055154	0.070854	0.06054
R (diff_$\rho_{F_{LeBail}+G}^{MEM}$)	0.1663	0.096320	0.08235
R (diff_$\rho_{F_{LeBail}+CF+G}^{MEM}$)	0.1984	0.108683	0.0949
R (diff_$\rho_{F_{obs}+CF+G}^{MEM}$)	0.2005	0.082994	0.08857

24-fold disordered oxalate anion which is rotated around an axis perpendicular to the principal axis in addition to having rotated carboxyl groups, thus leading to a quasi-spherical entity. The C—C bond of the anion is diagonally oriented with respect to the *ab* plane leading to 12-fold disorder, which is doubled by a mirror plane perpendicular to the *c* axis. The
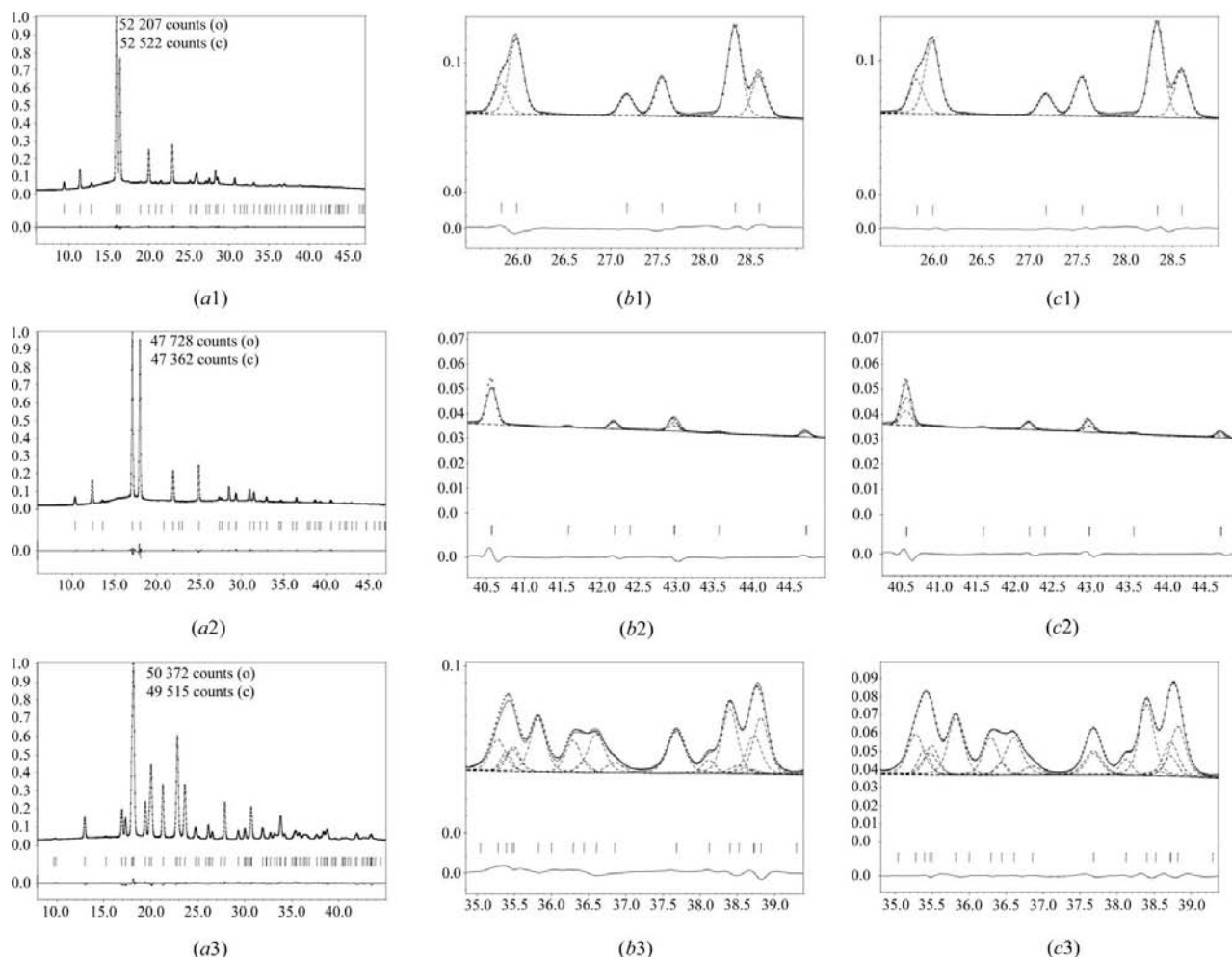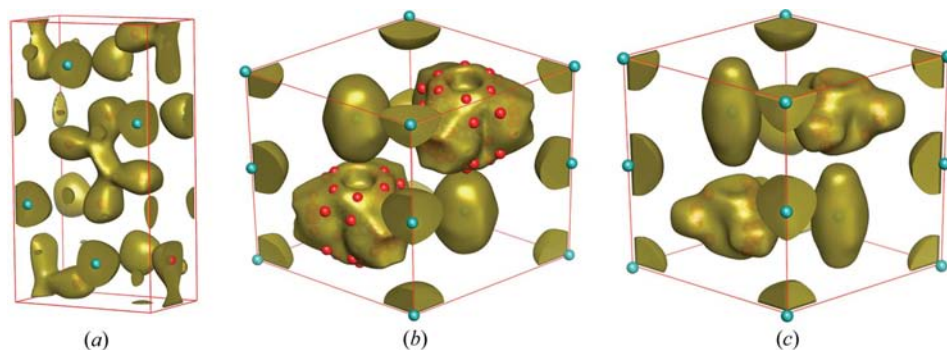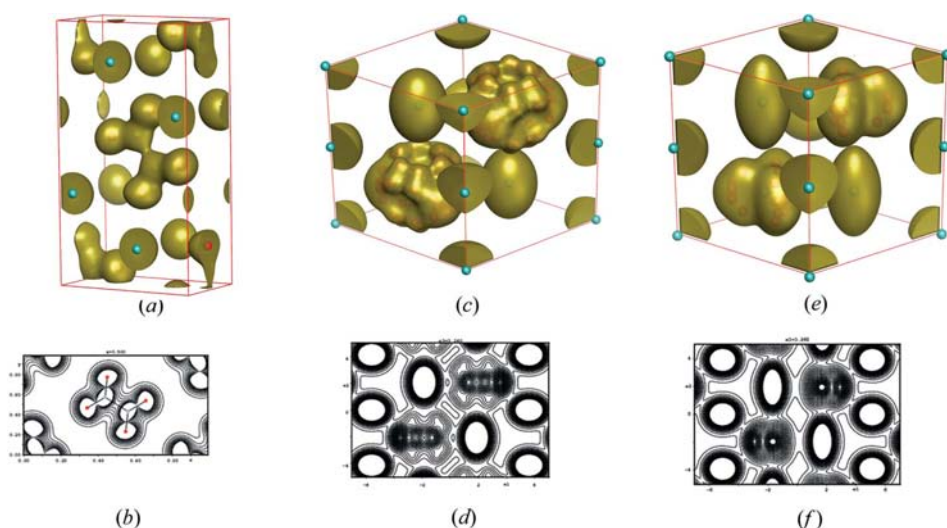

Figure 3
(*a*) Rietveld plots for α-Rb$_2$C$_2$O$_4$, α-Rb$_2$CO$_3$ and δ-K$_2$C$_2$O$_4$. Selected regions of (*b*) Rietveld and (*c*) Le Bail plots of the powder patterns of (*a*) showing overlapping reflections and their decomposition.

Figure 4
Electron densities obtained by charge flipping for (a) δ-$K_2C_2O_4$ (iso-level 2.5 e Å^{-3}); (b) α-$Rb_2C_2O_4$ (iso-level 0.25 e Å^{-3}); (c) α-Rb_2CO_3 (iso-level 0.6 e Å^{-3}). Colored spheres represent atomic positions of the Rietveld model.

Figure 5
Perspective views and corresponding two-dimensional projections of the procrystal electron densities of ordered δ-$K_2C_2O_4$ at 295 K (a), (b), disordered α-$Rb_2C_2O_4$ at 683 K (c), (d), and disordered α-Rb_2CO_3 at 873 K (e), (f). The following parameters have been used: (a) iso-level 1.0 Å^{-3}, volume/area = 30.1/142.2 ($\text{Å}^3/\text{Å}^2$); (b) projection along [001], contours 0.2 e Å^{-3}, cut-off at 2.5 e Å^{-3}, schematized oxalate dianion; (c) iso-level 0.6 Å^{-3}, volume/area = 95.56/250.930 ($\text{Å}^3/\text{Å}^2$); (d) projection along [110], contours 0.1, cut-off 3 e Å^{-3}; (e) iso-level 0.6, volume/area = 63.85/195 ($\text{Å}^3/\text{Å}^2$); (f) projection along [110], contours 0.1, cut-off 3 e Å^{-3}. Colored spheres represent atomic positions of the Rietveld model.

tures of α-$Rb_2C_2O_4$ and δ-$K_2C_2O_4$ (Fig. 3). The oxalate molecular anion was defined in a Cartesian coordinate system assuming the point group 222 as the internal symmetry of the anion with the C—C bond aligned along a twofold axis. The torsion angle, isotropic a.d.p.s of O and C atoms as well as anisotropic a.d.p.s for the rubidium cations were subjected to Rietveld refinement.

3.3. Charge flipping

Phases of reflections were reconstructed by the charge-flipping (CF) algorithm (Oszlányi & Sütő, 2004, 2005; Palatinus, 2004) combined with the method of histogram matching for repartitioning of the overlapping reflections (Zhang & Main, 1990; Baerlocher *et al.*, 2007). The structure factors were extracted by the Le Bail method. All calculations of CF were performed starting from random phases using the computer program *Superflip* (Palatinus & Chapuis, 2007). The method of the low-density elimination (LDE; Shiono & Woolfson, 1992) was used from the beginning of the calculations for the three structures to modify the density in real space. The histogram-matching method was used to repartition the overlapping reflections only in case of the disordered crystal structures (Figs. 4b and c). The histogram was created according to the chemical composition of the unit-cell content, taking into account the number of formula units per unit cell. A value of 0.2 for the parameter 'weak-ratio' was found to give the best performance. We also found that the histogram-matching method did not work well in the case of heavily overlapping reflections, and led to divergence. However, the low-density elimination method (LDE) already has the ability to reconstruct the phases of the model (Fig. 4a).

Comparison of the reflection phases resulting from CF with the phases corresponding to the structure models obtained by Rietveld refinements for the three structures shows that among 86/51/44 reflections for δ-$K_2C_2O_4$/α-$Rb_2C_2O_4$/α-

refined orientation of the oxalate dianion deviates from the ideal staggered conformation by approximately 12°. Since the mobility of the cations increases considerably with temperature, anisotropic a.d.p.s must be introduced. The crystal structure of α-Rb_2CO_3 (Fig. 2b) is isotypic to that of α-$Rb_2C_2O_4$ except for the fact that the carbonate group has no internal degree of freedom leading to pure orientational disorder. Crystallographic data for all three phases are listed in Table 1.

3.2. Rietveld refinements with local site symmetry

Pseudo-rigid-body Rietveld refinements were performed using *JANA*2000 (Petricek *et al.*, 2000) for the crystal struc-

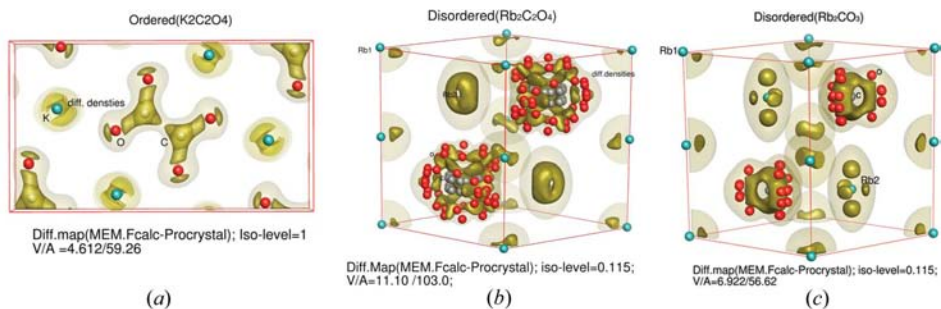**Figure 6**
Difference electron densities: $\rho_{calc}^{MEM} - \rho^{procrystal}$ for the crystal structures of ordered δ-$K_2C_2O_4$ in (a) and disordered α-$Rb_2C_2O_4$, α-Rb_2CO_3 in (b) and (c). Colored spheres represent atomic positions of the Rietveld model.

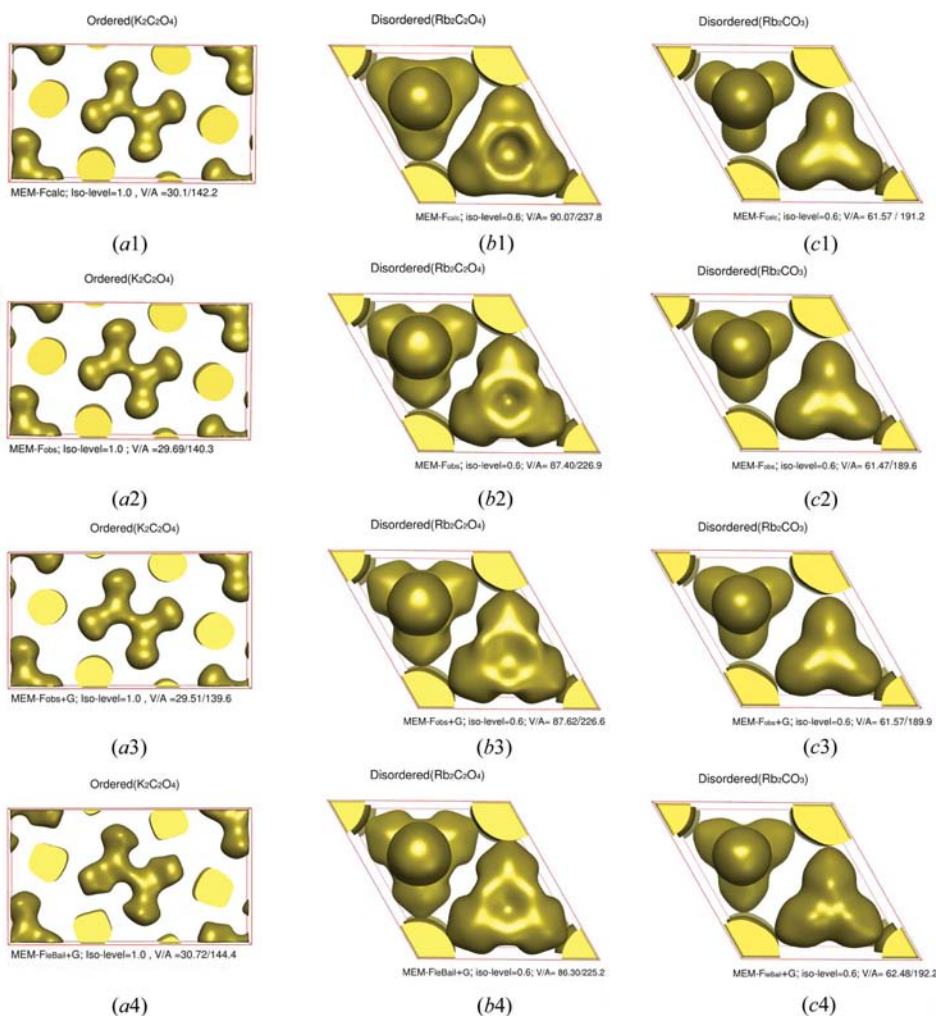**Figure 7**
MEM electron-density maps for the crystal structures of ordered δ-$K_2C_2O_4$ in (a) and disordered α-$Rb_2C_2O_4$, α-Rb_2CO_3 in (b) and (c) with different data subsets of F_{calc} (a1, b1, c1), F_{obs} (a2, b2, c2), F_{obs} + G constraints (a3, b3, c3) and F_{LeBail} + G constraints (a4, b4, c4). The iso-levels and the values of volume and area of the densities surfaces at the special iso-surfaces are displayed.

Rb_2CO_3 only 6/4/4 mismatches between the signs of the reflection phases exist for these centrosymmetric structures. All of these reflections are weak (supplementary data, Tables

S3, S4 and S5[1]). However, the resultant electron densities are not sufficiently accurate for the investigation of details of the crystal structures (Fig. 4): the reconstructed electron densities are affected by inaccurate estimates of the structure-factor amplitudes, possible errors of the scale factors and the series termination effect in the Fourier transforms. Despite these drawbacks, CF is a fast method to reconstruct the approximate image of the electron density using only the lattice parameters and the values of structure-factor amplitudes taken from a Le Bail fit.

3.4. MEM calculations

Calculations according to the MEM were performed with the computer program *BayMEM* (van Smaalen *et al.*, 2003), employing the Sakato–Sato algorithm (Sakata *et al.*, 1990) and a uniform prior electron density (ρ_i^{prior} = constant). Unit weights were used. Optimal values for the Lagrange multiplier λ_{FG} were obtained by trial and error. Values of λ_{FG} that were very small initially were increased until each step of the iteration involved a decrease of the value of the constraint by 10%. Too small values of λ_{FG} lead to very slow convergence. Too large values of λ_{FG} reveal themselves through divergence of the iterative procedure or at least an increase of the constraint value for several cycles of the iteration. The latter type of densities are unreliable and were not used. We found that a starting value of λ = 0.05 yielded the best convergence for all three data sets; an automated adjustment of λ during iterations was

---

[1] Supplementary data for this paper are available from the IUCr electronic archives (Reference: KD5036). Services for accessing these data are described at the back of the journal.

Table 3

Observed ($G_{obs}|F_{obs}$ and $G_{LeBail}|F_{LeBail}$) and MEM-reconstructed ($G_{MEM}|F_{MEM}$) structure factors for reflections in four selected G groups.

Results of two MEM calculations on α-Rb$_2$CO$_3$ are given: F_{obs} with φ^{CF} (A in Fig. 1) and F_{LeBail} with φ^{CF} (B in Fig. 1).

hkl	F_{obs} + G constraint		F_{LeBail} + G constraint	
	$G_{obs}|F_{obs}$	$G_{MEM}|F_{MEM}$	$G_{LeBail}|F_{LeBail}$	$G_{MEM}|F_{MEM}$
	11.54508	11.37630	11.25819	11.063571
205	1.42180	1.39721	11.41853	0.389331
4$\bar{1}$2	14.10400	13.89800	11.17715	13.54725
	8.14108	8.576332	7.655055	7.851617
106	7.00589	6.948771	7.869980	5.940244
401	−9.13630	−9.940902	−7.433918	−9.38132
	4.84396	4.450077	4.675526	5.212715
3$\bar{1}$5	0.00000	0.233524	4.711191	1.771974
402	8.39000	7.700681	4.603366	8.673950
	5.34194	4.983846	5.000933	4.750375
206	5.12069	4.988064	4.949198	4.828800
5$\bar{2}$1	−5.44920	−4.981735	−5.026601	−4.71067

allowed for α-Rb$_2$CO$_3$ (Table 2). Observed structure-factor amplitudes were obtained up to the experimental limit of $\sin(\theta)/\lambda = 0.78630$ Å^{-1} by model-biased decompositions from the final Rietveld refinements. Phased observed structure factors F_{obs} were then derived according to the procedure of Bagautdinov *et al.* (1998), and were used in the F constraints. The group amplitudes of groups of overlapping reflections (G amplitude) were calculated from the structure factors according to (5) with standard uncertainties (σ group) according to (6). These values were used in the G constraints. Alternatively, structure-factor amplitudes extracted from Le Bail fits were scaled according to the absolute scale of the Rietveld refinement. The structure factors obtained from Le Bail fit F_{LeBail} were corrected for the anomalous scattering effect according to the same procedure which is used for the

correction of F_{obs}, *i.e.* applying the ratio of $F_{calc}(hkl$, without AS)$/F_{calc}(hkl$, with AS), where AS is the anomalous scattering effect. Very small changes in the values of F_{LeBail} were thus found, which is reasonable because of the small anomalous scattering contributions (Rb has $f'' = 0.66$ and K has $f'' = 0.54$). The effects of possibly erroneous scale factors were tested by additional calculations employing scale factors larger and smaller by 5%. Despite minor differences in the densities, the main features of the disorder remained unaffected. Electron densities from *BayMEM* were reformatted in the unformatted ASCII file type of *X-PLOR*, and three-dimensional visualizations were produced by the *UCSF* software Chimera (Pettersen *et al.*, 2004). A small *Fortran* program was written for the calculation of the difference densities in three-dimensions.
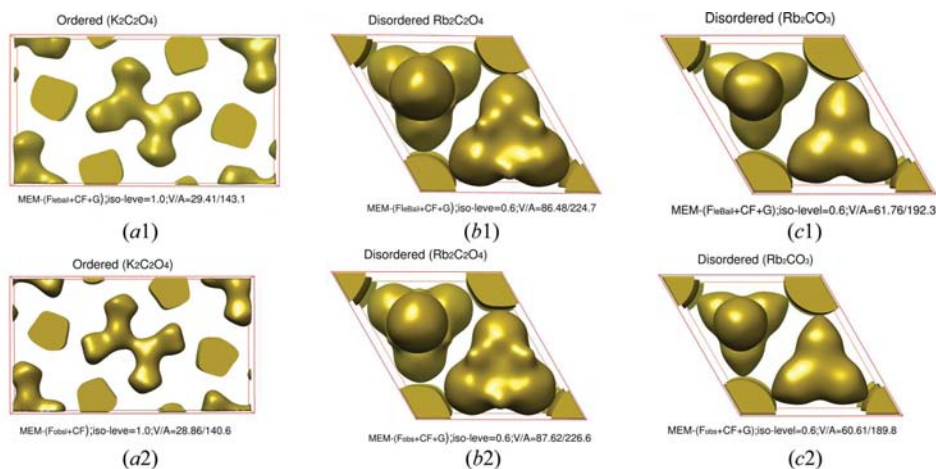
4. Electron densities

4.1. Procrystal density

Electron densities corresponding to the refined structure models (the procrystal densities $\rho^{procrystal}$; see §2.1) were calculated for the three compounds by the computer program *PRIOR* (van Smaalen *et al.*, 2003). The densities were sampled on a suitably fine grid (Table 2). Atomic positions and a.d.p.s were used from the final rigid-body Rietveld refinements (§3.2 and Table 1). Selected sections of the densities were visualized by contour plots generated with *JANA*2000, and three-dimensional visualizations were produced with the computer program *Chimera* (Pettersen *et al.*, 2004; Fig. 5). It is worth noting that this type of density map provides an approximation to the real electron density, while deformations of the electron density due to chemical-bonding effects or disorder beyond the model are not considered. The procrystal density has been used as a reference model for MEM calculations and to visualize structural differences between MEM densities and the procrystal structure.

4.2. MEM densities based on full-pattern fitting of the data

The MEM densities ρ_{calc}^{MEM} have been calculated with F constraints based on the calculated structure factors F_{calc} of the structure models obtained by Rietveld refinement (Fig. 1). This type of map should reproduce the structure model, but differences will occur because of series termination effects, *i.e.* structure factors have been used up to the experimental limit of $\sin(\theta)/\lambda = 0.7863$ Å^{-1} only. Furthermore, MEM densities may deviate from the true densities due to inadequacies of the MEM itself, in particular due to inadequacies related to the standard uncertain-

Figure 8
MEM electron densities of ordered δ-K$_2$C$_2$O$_4$ in (a) and disordered α-Rb$_2$C$_2$O$_4$, α-Rb$_2$CO$_3$ in (b) and (c) based on reflection phases from charge flipping with two different types of amplitudes. (a1), (b1), (c1) $|F_{LeBail}|$, and (a2), (b2), (c2) $|F_{obs}|$.

ties of the structure factors and the choice of weights in the F constraints [see (3)]. The differences between reconstructed and true densities can be analyzed by consideration of the difference densities $\rho_{calc}^{MEM} - \rho^{procrystal}$, as shown in Fig. 6.

Figure 9
Difference MEM electron densities: $(\rho_{(I)}^{MEM} - \rho_{calc}^{MEM})$ of ordered δ-K$_2$C$_2$O$_4$ in (ai) and disordered α-Rb$_2$C$_2$O$_4$, α-Rb$_2$CO$_3$ in (bi) and (ci), where $i = 1$ refers to F_{obs} (first row), $i = 2$ refers to F_{obs} with G constraints (second row) and $i = 3$ refers to F_{LeBail} with G constraints (last row). Colored spheres represent atomic positions of the Rietveld model.
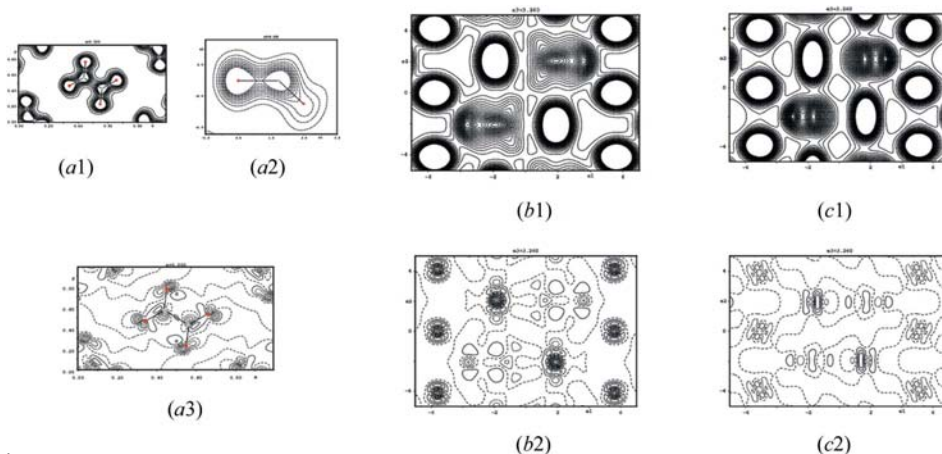
Figure 10
Two-dimensional sections of MEM and difference MEM maps based on F_{obs}–G constraints for the three structures. ($a1$) and ($a2$) are sections along and perpendicular (includes only C and O atoms) to the mirror plane containing the planar oxalate dianion; contours are drawn at 0.5 e Å^{-3} with a cut-off of 5 e Å^{-3}. ($a3$) is a section along the 002 plane of the difference MEM density; contours are at 0.15 e Å^{-3}. ($b1$, $b2$) and ($c1$, $c2$) are sections parallel to the 110 plane for the MEM map (contour lines at 0.1 and cut-off 3 e Å^{-3}) and difference MEM maps [+ ve (solid lines), −ve (dashed lines) contours are at 0.15 e Å^{-3}] for rubidium oxalate and rubidium carbonate.

Although the difference densities are small (real-space agreement factors between ρ_{calc}^{MEM} and ρ^{pro} are $R = 0.0598$ for α-Rb$_2$C$_2$O$_4$ and $R = 0.0416$ for α-Rb$_2$CO$_3$), they can be of the same order of magnitude as the effects being studied. Under the assumption that series-termination effects and other errors will have similar values in different maps, we have employed ρ_{calc}^{MEM} as a reference density for analyzing the differences between the various experimental MEM densities and the density of the IAM model. This assumption is justified by the fact that all MEM maps have been obtained with data up to the same resolution and with the same standard uncertainties and the same weighting scheme.

The MEM densities have been calculated with F constraints based on the phased observed structure factors F_{obs} [Figs. 1, 7($a2$), ($b2$) and ($c2$)]. Especially in the case of powder diffraction data this kind of map is biased by the model, because calculated structure factors of the model are used to decompose overlapping reflections into contributions of individual reflections. The number of overlapping reflections is small for the two disordered structures, but it is larger for the lower-symmetry structure δ-K$_2$C$_2$O$_4$. Therefore, additional MEM densities have been calculated with F constraints based on the phased observed structure factors F_{obs} of well resolved reflections and G constraints based on the group amplitudes of overlapping reflections (Fig. 1). The densities ρ_{obs+G}^{MEM} are given in Figs. 7($a3$), ($b3$) and ($c3$). The capability of the MEM to reconstruct the values of structure-factor amplitudes and their phases of individual reflections from the G constraint is illustrated in Table 3 for four overlap groups in the diffraction data of α-Rb$_2$CO$_3$.

Unbiased observed structure-factor amplitudes are those extracted from Le Bail fits to the diffraction data, *i.e.* by a Le Bail decomposition disregarding any
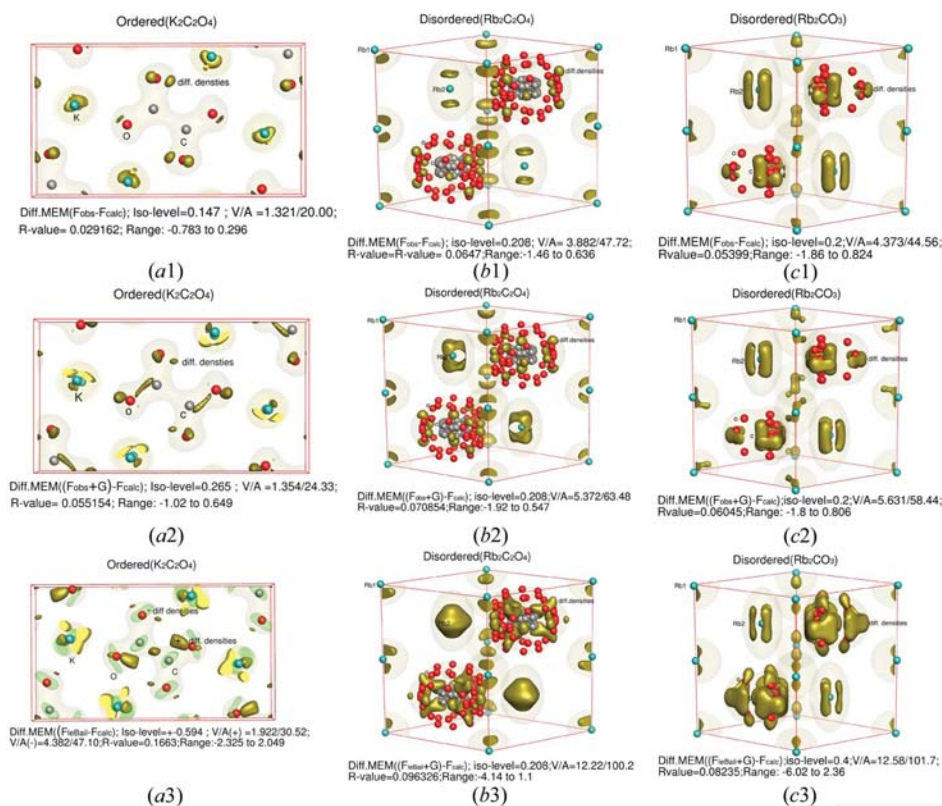
structural information. This procedure provides amplitudes as they would have been directly measured by single-crystal diffraction, except that the Le Bail procedure can only provide accurate amplitudes for resolved reflections. For each group of overlapping reflections an accurate value is obtained for the sum of intensities. Therefore, useful MEM calculations can only be performed with a combination of F and G constraints, resulting in the densities $\rho_{\mathrm{LeBail}+G}^{\mathrm{MEM}}$ [Figs. 1, 7(a4), (b4) and (c4)]. The fourth and fifth columns in Table 3 clearly show that the MEM has successfully partitioned the groups of overlapping reflections into contributions of individual reflections and that the MEM leads to the same phases as have been obtained by charge flipping. For all four overlap groups the

two reflections have almost perfect overlap, the Le Bail decomposition has thus given nearly equal magnitudes for the structure factors of the two reflections in each group (Table 3).

4.3. MEM densities based on charge flipping

The phased observed structure factors obtained after Rietveld refinement are biased towards the structure model for their amplitudes, while they have phases defined by the model. A model-independent estimate of the reflection phases is obtained by charge flipping, resulting in the set of phases φ_{CF}. MEM densities have been calculated for the combinations of observed structure-factor amplitudes $|F_{\mathrm{obs}}|$ with φ_{CF} and of Le Bail-extracted amplitudes $|F_{\mathrm{LeBail}}|$ with φ_{CF} (Fig. 1). Combinations of F and G constraints have been used, except in the case of potassium oxalate, which is based exclusively on the F constraint (Table 2). The resulting densities are given in Fig. 8.

Figure 11
Difference MEM electron densities: ($\rho_{(\mathrm{I})}^{\mathrm{MEM}}$) of ordered δ-K$_2C_2O_4$ in (ai) and disordered α-Rb$_2$C$_2$O$_4$, α-Rb$_2$CO$_3$ in (bi) and (ci), where $i = 1$ refers to F_{LeBail} (first row) and $i = 2$ refers to F_{obs} (second row). In both cases the phases obtained from CF and applying G constraints for the three compounds. Colored spheres represent atomic positions of the Rietveld model.

5. Discussion

Six types of MEM electron-density maps have been calculated for three compounds with related crystal structures. The MEM densities vary in the amount of bias towards the structure models, which affects the amplitudes and phases of the structure factors. The completely biased densities $\rho_{\mathrm{calc}}^{\mathrm{MEM}}$ (Fig. 1) give an indication of the amount of information that can be extracted by the MEM from the data. Comparison of $\rho_{\mathrm{calc}}^{\mathrm{MEM}}$ [Figs. 7(a1), (b1) and (c1)] with the corresponding model densities [Figs. 5(a)–(f)] shows that the latter are much more structured than the former, especially in the cases of the oxalates. This strongly suggests that the highly structured densities of the models are actually artifacts. A smooth character is also found for the MEM densities based on the experimental data (Figs. 7 and 8). Differences with $\rho_{\mathrm{calc}}^{\mathrm{MEM}}$ can be analyzed on the basis of difference densities
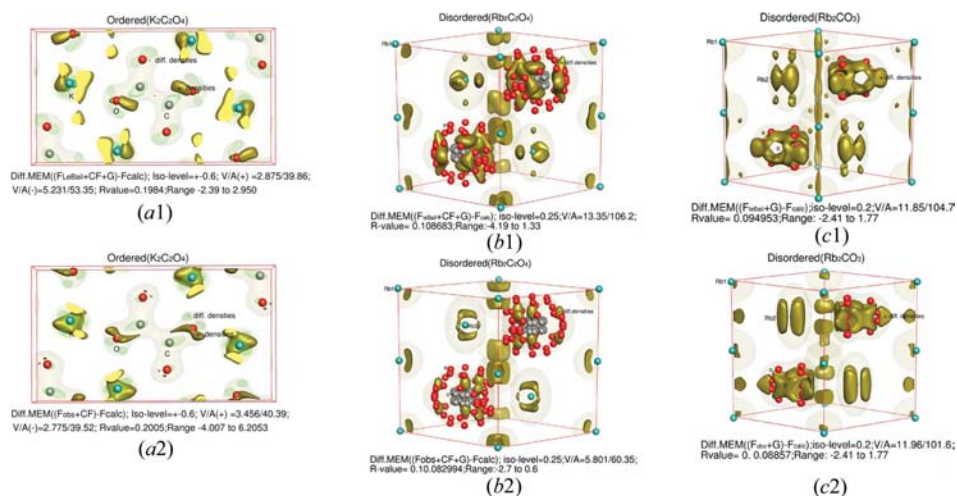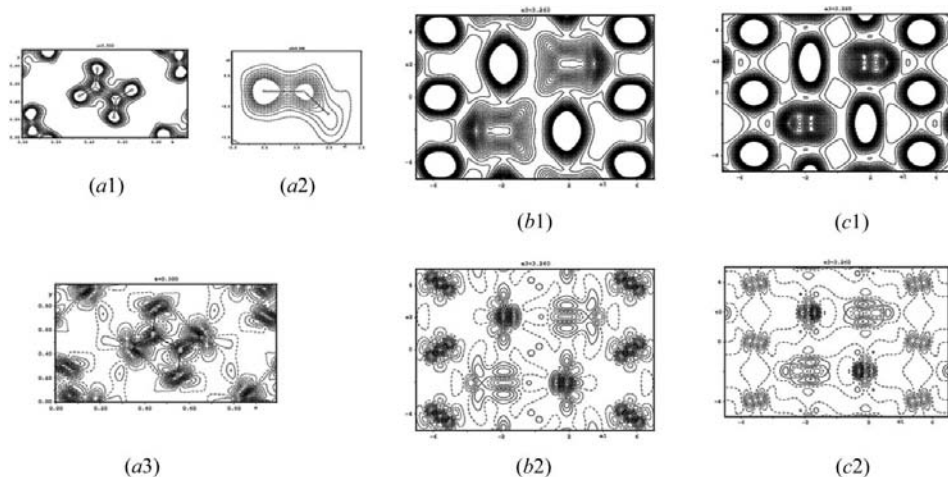

Figure 12
Two-dimensional sections of the MEM and difference-MEM maps based on F_{LeBail}–G constraints and phases from CF for the three compounds. (a1) and (a2) show sections along and perpendicular (includes only C and O atoms) to the mirror plane containing the planar oxalate anion. Contours are at 0.5 with a cut-off of 5 e Å^{-3}. (a3) is a section along the 002 plane for the difference MEM, contour lines at 0.15 e Å^{-3}. (b1, b2) and (c1, c2) are the sections along the 110 plane for the MEM map (contour lines at 0.1 e Å^{-3} with a cut-off of 3 e Å^{-3}) and difference MEM maps [+ ve (solid lines), −ve (dashed lines) contours are drawn at 0.15 e Å^{-3}] for rubidium oxalate and rubidium carbonate.

$$\Delta\rho_{(I)}^{\mathrm{MEM}} = \rho_{(I)}^{\mathrm{MEM}} - \rho_{\mathrm{calc}}^{\mathrm{MEM}}, \qquad (8)$$

where (I) stands for one of the six types of maps: obs, obs + G, Le Bail + G, obs + CF, obs + CF + G and Le Bail + CF + G (Fig. 1). The differences are visualized by plots of iso-surfaces of $\Delta\rho_{(I)}^{\mathrm{MEM}}$ (Figs. 9–12) and they are quantified by the area and volumes of these iso-surfaces as well as by the real-space R value of matching $\rho_{(I)}^{\mathrm{MEM}}$ and $\rho_{\mathrm{calc}}^{\mathrm{MEM}}$ (Table 2). The values for the volume and the area of the iso-surfaces are calculated in a way that the iso-surface value of the difference-MEM map is changed until the density level reaches the densities of the MEM map. This procedure of choosing the iso-surface of difference-MEM maps is used because of the huge differences between the ranges of the difference-MEM maps. This holds especially true when the data originate from Le Bail fits of different uncertainty values, compared with Rietveld refinement. Fig. 7 presents comparative considerations of the electron densities of the three compounds with different data subsets as calculated above; the enclosed volume and area of the iso-surfaces are indicated in the maps. For each compound all four maps have similar appearances, but significant differences are also found between any MEM density and the corresponding reference MEM density based on F_{calc}. These differences can be visualized by difference maps (Fig. 9). Analysis of $\Delta\rho_{\mathrm{obs}}^{\mathrm{MEM}}$, $\Delta\rho_{\mathrm{obs}+G}^{\mathrm{MEM}}$ and $\Delta\rho_{\mathrm{LeBail}+G}^{\mathrm{MEM}}$ leads to the following observations:

(i) In the case of the ordered crystal structure of δ-K$_2$C$_2$O$_4$, non-zero values of difference densities $\Delta\rho_{(I)}^{\mathrm{MEM}}$ are restricted to small regions in space. Although the differences can be relatively high, this indicates that the MEM confirms the structure model in most aspects. Observed features in $\Delta\rho_{(I)}^{\mathrm{MEM}}$ can be artifacts but will also include features due to an inadequate description of thermal motion in the model. The latter interpretation is supported by the fact that differences increase on going from F_{obs} to $F_{\mathrm{obs}} + G$ to $F_{\mathrm{LeBail}} + G$ in the MEM calculation. Large displacements are found for the O atoms in directions out of the mirror plane (Fig. 10a2).

(ii) For the disordered, high-temperature phase of α-Rb$_2$C$_2$O$_4$, the range of values of $\Delta\rho_{(I)}^{\mathrm{MEM}}$ is similar as for ordered δ-K$_2$C$_2$O$_4$, but the regions of appreciable difference are much larger than in the ordered case. This finding suggests that the model has not captured the disorder with the same precision that is possible for an ordered structure. In addition to the orientational and conformational disorder of the oxalate anions, $\Delta\rho_{(I)}^{\mathrm{MEM}}$ clearly shows the mobility of the cations. The displacements of Rb2 along the c axis are larger than those of Rb1, as is most clearly seen in the (110) sections of $\rho_{(I)}^{\mathrm{MEM}}$ and $\Delta\rho_{(I)}^{\mathrm{MEM}}$ [Figs. 10(b1) and (b2)] .

(iii) For the disordered, high-temperature phase of α-Rb$_2$CO$_3$, the same conclusions are obtained as for disordered α-Rb$_2$C$_2$O$_4$, but with larger displacements for Rb2 along the c axis compared with Rb2 in α-Rb$_2$C$_2$O$_4$ [Figs. 10(c1) and (c2)].

A new combination of MEM and CF is presented here. Phases from CF are combined with either the observed structure factors from Rietveld refinements or the observed structure factors obtained by the Le Bail procedure (Fig. 1). The first conclusion is that for all three compounds the main

features of the densities are also reproduced by these two maps (Figs. 7 and 8). Turned around, this implies that the completely model-free approach of charge-flipping with Le Bail fitting provides a reasonable-to-good description of the crystal structure, including features due to disorder. Nevertheless, $\Delta\rho_{(I)}^{\mathrm{MEM}}$ show significant differences between model and MEM densities:

(iv) For ordered δ-K$_2$C$_2$O$_4$, MEM densities are deformed [Figs. 8(a1) and (a2)] compared with the previous MEM calculations, which is reflected in the high values of the agreement factor (R = 0.2005 and 0.1984) in both cases of combinations.

(v) For the disordered crystal structures of α-Rb$_2$C$_2$O$_4$ and α-Rb$_2$CO$_3$, the agreement factors are slightly higher for the MEM maps obtained by the combinations Le Bail + G, obs + CF + G, and Le Bail + CF + G compared with the maps derived from obs and obs + G (Table 2). It therefore seems that the use of Le Bail amplitudes and CF phases is particularly successful in the case of partially ordered structures, $i.e.$ in the case of densities that are relatively smooth compared with the peaked densities of well located atoms.

6. Conclusions

The electron densities of ordered δ-K$_2$C$_2$O$_4$, and disordered α-Rb$_2$C$_2$O$_4$ and α-Rb$_2$CO$_3$ have been successfully reconstructed from X-ray powder diffraction data by the maximum entropy method (MEM). The MEM has been applied in a series of calculations ranging from calculations completely biased by the model to model-free calculations. The first observation is that for each compound all MEM calculations lead to similar densities; the MEM calculations give good representations of the crystal structure including disorder and anharmonic atomic displacements (Figs. 7 and 8). In particular, this implies that crystal structures including positional and orientational disorder of functional groups can be determined from X-ray diffraction data without the need for a structure model: structure-factor amplitudes are obtained by Le Bail fits to the diffraction data and structure-factor phases are determined by charge flipping with histogram matching.

The MEM employs phased structure factors as input (F constraint), while part of the diffraction information can be available as sums of intensities of groups of overlapping reflections (G constraint) as is typically available from powder diffraction. The MEM with F_{obs} as 'experimental data' (structure-factor phases from the model and structure-factor amplitudes by Le Bail decomposition biased by the model) leads to densities that differ by the least amount from the model. Stepwise replacement of more of the models by experimental-based information leads to increasing differences to the model densities (Figs. 9–12). Part of these differences will be due to inaccurate values for amplitudes or phases of reflections or to intrinsic features of the MEM related to the use of the G constraint. However, another part these differences will reflect anisotropic atomic displacement parameters (ordered δ-K$_2$C$_2$O$_4$) not used in the model, and

they indicate better representations of the disorder in α-$Rb_2C_2O_4$ and α-Rb_2CO_3 by the MEM than is given by the models.

The most important result is that completely *ab initio* electron-density distributions have been obtained by the MEM applied to the combination of structure-factor amplitudes from Le Bail fits with phases from charge flipping. This new combination of the MEM and the method of charge flipping can thus be used for the determination of partially ordered crystal structures from powder diffraction data.

References

Baerlocher, Ch., McCusker, L. B. & Palatinus, L. (2007). *Z. Kristallogr.* **222**, 47–53.

Bagautdinov, B., Luedecke, J., Schneider, M. & van Smaalen, S. (1998). *Acta Cryst.* B**54**, 626–634.

David, W. I. F., Shankland, K., McCusker, L. B. & Baerlocher, C. (2002). Editors. *Structure Determination from Powder Diffraction Data.* Oxford University Press.

Dinnebier, R. E., Schneider, M., van Smaalen, S., Olbrich, F. & Behrens, U. (1999). *Acta Cryst.* B**55**, 35–44.

Dinnebier, R. E., Vensky, S., Jansen, M. & Hanson, J. C. (2005). *Chem. Eur. J.* **11**, 1119–1129.

Oszlányi, G. & Sütő, A. (2004). *Acta Cryst.* A**60**, 134–141.

Oszlányi, G. & Sütő, A. (2005). *Acta Cryst.* A**61**, 147–152.

Oszlányi, G. & Sütő, A. (2007). *Acta Cryst.* A**63**, 156–163.

Palatinus, L. (2004). *Acta Cryst.* A**60**, 604–610.

Palatinus, L. & Chapuis, G. (2007). *J. Appl. Cryst.* **40**, 786–790.

Palatinus, L. & van Smaalen, S. (2002). *Acta Cryst.* A**58**, 559–567.

Petricek, V., Dusek, M. & Palatinus, L. (2000). *JANA*2000. Institute of Physics, Praha, Czech Republic.

Pettersen, E. F., Goddard, T. D., Huang, C. C., Couch, G. S., Greenblatt, D. M., Meng, E. C. & Ferrin, T. E. (2004). *J. Comput. Chem.* **25**, 1605–1612.

Sakata, M., Mori, R., Kumazawza, S., Takata, M. & Toraya, H. (1990). *J. Appl. Cryst.* **23**, 526–534.

Shiono, M. & Woolfson, M. M. (1992). *Acta Cryst.* A**48**, 451–456.

Takata, M. (2008). *Acta Cryst.* A**64**, 232–245.

Takata, M. & Sakata, M. (1996). *Acta Cryst.* A**52**, 287–290.

Takata, M., Umeda, B., Nishibori, E., Sakata, M., Saito, Y., Ohno, M. & Shinohara, H. (1995). *Nature (London)*, **377**, 46–49.

van Smaalen, S. (2007). *Incommensurate Crystallography.* Oxford University Press.

van Smaalen, S., Palatinus, L. & Schneider, M. (2003). *Acta Cryst.* A**59**, 459–469.

Vries, R. Y. de, Briels, W. J. & Feil, D. (1994). *Acta Cryst.* A**50**, 383–391.

Vries, R. Y. de, Briels, W. J. & Feil, D. (1996). *Phys. Rev. Lett.* **77**, 1719–1722.

Yamamoto, K., Takahashi, Y., Ohshima, K., Okamura, F. P. & Yukino, K. (1996). *Acta Cryst.* A**52**, 606–613.

Yashima, M. & Tsunekawa, S. (2006). *Acta Cryst.* B**62**, 161–164.

Zhang, K. Y. J. & Main, P. (1990). *Acta Cryst.* A**46**, 41–46.